Ultrasound-induced changes in mesostructure of amorphous iron (III) hydroxide xerogels: A small-angle neutron scattering study

V. K. Ivanov,[1,2] G. P. Kopitsa,[3] F. Yu. Sharikov,[4] A. Ye. Baranchikov,[1,2] A. S. Shaporev,[1] S. V. Grigoriev,[3] and P. Klaus Pranzas[5]

[1]*Institute of General and Inorganic Chemistry, Moscow 119991, Russia*

[2]*Moscow State University, Moscow 119992, Russia*

[3]*Petersburg Nuclear Physics Institute, Gatchina 188300, Russia*

[4]*Federal State Unitary Enterprise Russian Scientific Center "Applied Chemistry," St. Petersburg 197198, Russia*

[5]*GKSS Research Centre, Geesthacht, Germany*

(Received 3 April 2008; revised manuscript received 16 February 2010; published 5 May 2010)

Structure and thermal properties of iron (III) hydroxide xerogels obtained under high intensity ultrasonic treatment were studied by means of small-angle neutron scattering and heat-flux calorimetry. It was established that sonication affects the mesostructure of amorphous xerogels (i.e., increase in their homogeneity, surface fractal dimension, and the sizes of aggregates of primary particles) as opposed to the commonly accepted point of view that ultrasonic action cannot lead to notable changes in structure of powders, consisting of nanometer size particles. Ultrasonically induced structural changes in xerogels are evidently confirmed via their notably different reactivity at thermal decomposition under hydrothermal conditions.

DOI: 10.1103/PhysRevB.81.174201 PACS number(s): 61.43.Hv, 43.35.+d, 61.05.fg

I. INTRODUCTION

Acoustic waves of ultrasonic frequency (2×10^4–2×10^9 Hz) are widely used nowadays in material science, material processing, medicine, etc. High-frequency ultrasound ($>1\times10^6$ Hz) has become a common tool for nondestructive testing of materials and biological objects. Distinctive features of acoustic testing techniques are relatively high resolution (up to tenth micron), possibility of building three-dimensional images of a material under investigation and real time monitoring as well as simple sampling procedures. Low-frequency (2×10^4–2×10^6 Hz) acoustic waves are widely used for measurement of distances to hard-to-reach objects, so they find a large variety of applications in sonars, geoacoustics, and so on.

Recently considerable progress was achieved in the field of application of high intensity ultrasonic treatment to nanomaterials synthesis. In the last few years a number of papers and reviews devoted to the development of advanced sonochemical methods of nanopowders and nanocomposites preparation were published.[1–4]

Specific physical and chemical effects taking place during sonication of liquids arise mostly from acoustic cavitation, i.e., formation of vapor-gas microbubbles and their further oscillations and collapse. It should be noted that the mechanism of sonochemical reactions in homogeneous liquids is well studied and thus obtained data are usually treated in the frames of two major theories, namely, hot spot theory[5] and the theory of local electrization.[6] The former is based on the thesis that high local temperatures (up to several thousand degrees) and pressures (several kilobars) arise during the collapse of cavitation bubbles. The latter explains the mechanism of sonochemical reactions through high local electric potentials formed on the surface of cavities leading to intensive electrical discharges. In both cases extreme conditions in cavities lead to decomposition of volatile constituents of the liquid (for instance, organometallic compounds, metal complexes, etc.) and formation of nanostructured products.

In turn, information on the specific action of high intensity ultrasound on heterogeneous systems (mainly liquid-solid systems) is still rather poor. It is generally accepted that the collapse of cavitation bubbles in the vicinity of the phase boundary (e.g., solid-liquid interface) occurs asymmetrically. Under these conditions the boundary is affected by shock-waves and local microjets of liquid. Thus, acoustic treatment of suspensions consisting of relatively large particles, which size is comparable to the size of a collapsing cavitation bubble ($d>0.5$–1 μm) leads to several specific effects including deagglomeration, decrease in mean particle size, increase in the surface area, etc.[3] Investigations concerning the influence of sonication on heterogeneous systems (for instance, sols and gels) consisting of substantially smaller particles were performed on a quite limited number of systems, including xerogels of zirconia[7] and silica.[8–10] It was established that ultrasonication leads to the increase in the rate of gel formation and to changes in the mesostructure (e.g., density, size of monomers, and size of aggregates) of hydrogels, xerogels, and aerogels. Nevertheless the effect of ultrasonication on such systems is to be studied more thorough.

In view of this circumstance this work aims to analyze the influence of high intensity ultrasound on the mesostructure of amorphous xerogels. Iron (III) hydroxide xerogels consisting of aggregated colloidal particles were chosen as a model system. Our investigation was primarily based on the use of small-angle neutron scattering (SANS) method which is widely used in the study of nuclear and magnetic inhomogeneities in various amorphous materials including xerogels, aerogels, etc.[11] SANS experiments had shown that ultrasonication unexpectedly results both in the increase in homogeneity of xerogels and in the increase in its fractal dimension. Additional information confirming these structural changes was obtained by means of *in situ* heat-flux calorimetry of hydrothermal decomposition of iron hydroxide samples and by analysis of iron oxide hydrothermally synthesized from initial $Fe(OH)_3$ xerogels.

The paper is organized in the following way. Section II describes the samples preparation and methods used in our work. The results of the SANS experiments are presented in Sec. III, dealing with investigations of the ultrasonically treated and nontreated xerogels mesostructure. The results of *in situ* calorimetric experiments showing the difference in kinetics of hydrothermal decomposition of ultrasonically treated and nontreated samples are given in Sec. IV. Section V contains a summary of results obtained.

II. EXPERIMENTAL

A. Preparation of the samples

Iron (III) hydroxide gels were precipitated from iron (III) nitrate solutions as follows: 50 ml of iron (III) nitrate aqueous solution (0.3 and 1.0 M) were added dropwise to 50 ml of ammonia aqueous solution (7.5 M) under vigorous stirring. The total duration of precipitation procedure was 15 min. Gels of iron (III) hydroxide were also precipitated under the same conditions but under ultrasonic treatment. Bandelin Sonopuls HD 3200 generator equipped with titanium horn and TT-13 tip was used as the source of acoustic vibrations. The ultrasonic vibration frequency was maintained equal to 20 kHz, the oscillation amplitude of the waveguide tip was 150 μm. The output power measured using standard calorimetric technique was 59 W/cm^2. Ultrasonic horn was immersed 10 mm below the surface of solutions. To prevent overheating the precipitation process was conducted in the cell thermostated at 25 °C.

Upon completion of the sedimentation procedure the suspensions of iron (III) hydroxide were additionally stirred for 30 min. Then iron (III) hydroxide gels were centrifuged (8000 min^{-1}) and washed several times with distilled water until the conductivity of mother liquor was lower than 0.3 mS. Conductivity was measured using Hanna HI 98312 conductometer with temperature compensation. Washed gels were dried in air at 60 °C for 12 h to produce iron (III) hydroxide xerogels. For the sake of clarity, the iron (III) hydroxide xerogels synthesized from 0.3 and 1 M solutions under ultrasonic treatment (US) and without it (C) are named hereafter Fe-0.3US, Fe-1US, Fe-0.3C, and Fe-1C, respectively.

Hydrothermal processing of the xerogels obtained was performed using Parr 4793 autoclave with PTFE liner (66 ml volume) equipped with Parr 4836 thermocontroller capable to maintain constant temperature in the solution with ±2 °C accuracy. 0.50 g of each xerogel sample was mixed with 40 ml of distilled water and heated up to 160 °C (heating rate β=2.25 °C/min), maintained at this temperature for 5 h and then cooled in air. Iron oxide obtained was centrifuged at 8000 rpm and dried in air at 60 °C for 12 h. Hereafter iron oxide samples obtained from Fe-0.3US, Fe-1US, Fe-0.3C, and Fe-1C xerogels are named Fe-0.3USHT, Fe-1USHT, Fe-0.3CHT, and Fe-1CHT, respectively.

B. *In situ* heat-flux calorimetry

Calorimetric study of hydrothermal decomposition of sonicated and nonsonicated iron (III) hydroxide xerogels was performed using C80 SETARAM Calvet calorimeter in linear heating mode (β=0.5 °C/min) at 30–210 °C. Calorimetric experiments were run in stainless-steel high-pressure vessels (8.5 cm^3) directly under hydrothermal conditions. Each xerogel powder was loaded into the vessel, then distilled water was added, and suspension was mechanically mixed for 3 min. After that the vessel was closed and inserted into the calorimetric block to perform a run.

Temperature calibration for the experimental vessels used was carried out against melting points of reference substances (gallium-indium-tin). Dynamic calibration was performed for Joule effect with the special calibration cell and additionally verified against melting heat effects of the same reference substances. Additional details on the calorimetric measurements procedure, deconvolution procedure, data processing, and their preparation for kinetic analysis are described elsewhere.[12,13]

C. Thermal analysis, XRD, and transmission electron microscopy (TEM) study of the samples

Thermal analysis [thermogravimetric analysis/differential thermal analysis (DTA)] of iron (III) hydroxide xerogels was performed using Pyris Diamond thermoanalyzer (Perkin-Elmer) in the temperature range 20–900 °C (heating rate β=10°/min) in air. X-ray diffraction (XRD) patterns of iron (III) hydroxide and iron (III) oxide samples were recorded using Rigaku D/MAX 2500 diffractometer (Cu K_α radiation). Analysis of microstructure of the samples was performed using Leo 912 AB Omega transmission electron microscope.

D. Neutron measurements

SANS measurements were performed on SANS-2 setup (FRG1 neutron reactor, GKSS Research Centre, Geesthacht, Germany), which operates in geometry close to a point geometry. The experiments were performed at neutron wavelengths λ=5.8 and 11.6 Å with $\Delta\lambda/\lambda$=10% and for four sample-detector distances SD=1, 3, 9, and 20.7 m, which allowed to perform the measurements of the neutron scattering intensity for momentum transfers in the range $8\times10^{-4} < q < 2.5\times10^{-1}$ $Å^{-1}$. The scattered neutrons were detected by a two-dimensional (2D) position-sensitive ^{3}He detector.

The samples of amorphous $Fe(OH)_3\cdot yH_2O$ xerogels were placed in a 1-mm-thick quartz cell, next samples were vibrocompacted using a standardized technique (vibration frequency 240 min^{-1} and amplitude 3 mm). Apparent density of each sample was calculated as a weight of a powder divided by its volume. The initial spectra for each q range were corrected using the standard procedure taking into account the scattering from the setup equipment and cell, as well as background. Resulting 2D isotropic spectra were averaged azimuthally and their absolute values were determined by normalizing to the incoherent-scattering cross section from vanadium with inclusion of the detector efficiency and apparent density ρ_H for each sample. All measurements were done at room temperature.

The SANS intensity analyzed hereafter was defined as

$$I_s(q) = I(q) - T \cdot I_0(q), \quad (1)$$

where $I(q)$ and $I_0(q)$ are the momentum-transfer distribution of the scattering neutrons behind the sample and beam without the sample, respectively, and $T=I/I_0=\exp(-\Sigma \cdot L)$ is the transmission coefficient of the neutrons passing through the sample, where Σ is the integral scattering cross section and L is the sample thickness. The setup resolution function was approximated by a Gaussian and was calculated separately for each distance SD with the use of the standard procedure.[14]

III. RESULTS OF SANS EXPERIMENT

In the present work we had studied the effect of power ultrasound on nanostructured systems on an example of amorphous iron hydroxide. Amorphous nature of all the forth analyzed samples was confirmed by means of XRD diffraction. According to thermal analysis data, total weight loss for all the samples is 24.8–26.5 %, that is very close to theoretical value for $Fe(OH)_3$ equal to 25.2%. Basing on these data we can conclude that the composition of all of these xerogels corresponds to iron (III) hydroxide containing a small amount of physisorbed water. Thus chemical formula of xerogels thus can be written as $Fe(OH)_3 \cdot yH_2O$ ($y \leq 0.1$).

Analysis of DTA curves allows one to conclude that the thermolysis of the xerogels regardless on concentration of initial solutions and application of ultrasound seems to proceed nearly identically. The first endothermic peak with maximum at ~120 °C can be attributed to the dehydration and the removal of both physisorbed and chemically bonded water. Next, a relatively weak exothermic peak with maximum at ~250 °C probably corresponds to decomposition of adsorbed nitrate ions and the last, strong exothermic peak at 400–410 °C not accompanied with a noticeable mass loss can obviously be ascribed to the crystallization of hematite (α-Fe_2O_3).

Figures 1 and 2 show the experimental curves of differential neutron cross section $d\Sigma(q)/d\Omega$ for amorphous iron (III) hydroxide xerogels precipitated from $Fe(NO_3)_3$ solutions of different concentrations without ultrasonic treatment (Fig. 1) and under sonication (Fig. 2). According to these figures, SANS intensity from the samples prepared from more concentrated solutions (1 M) in both cases is notably higher. This clearly indicates that (1) the nuclear density homogeneity of xerogels in the range 10–1000 Å is decreased with the increase in solutions concentration and (2) this situation is not changed upon sonication.

In SANS experiments for various materials, the power-law momentum-transfer dependence of the scattering intensity for such materials is usually observed in the form $I(q) \sim q^{-n} (n \leq 6)$ in a certain momentum-transfer region $q > 1/R$, where R is the characteristic scale of the scattering system. The fractal dimension of the system and the correlation function of scattering inhomogeneities are determined by the n value or, more precisely, by the deviation from the Porod asymptotic dependence ($n=4$). For volume and mass fractals, n coincides with the fractal dimension D_V, $1 \leq D_V \leq 3$. For the scattering from three-dimensional objects with

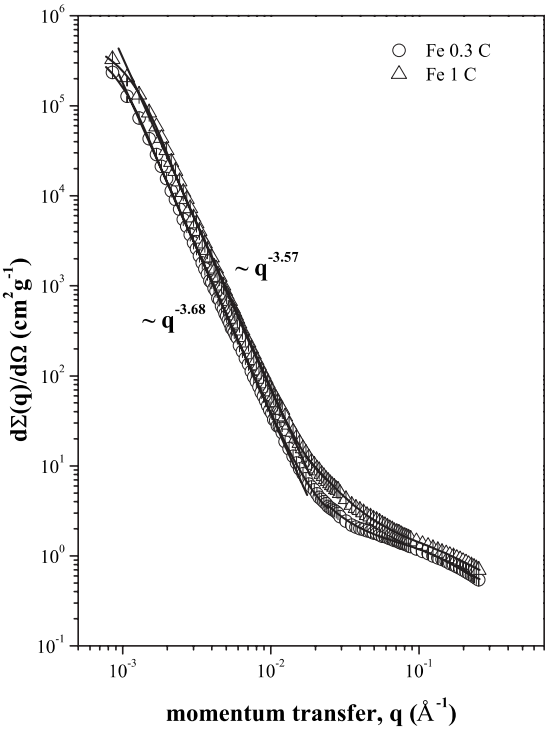

FIG. 1. SANS differential cross section $d\Sigma(q)/d\Omega$ for control (nonsonicated) samples of amorphous $Fe(OH)_3 \cdot yH_2O$ xerogels obtained from $Fe(NO_3)_3$ solutions of different concentrations. Description of experimental data with formula (2) is given with firm lines. Corresponding n values are also indicated as q^{-n}.

fractal surfaces $3 < n = 6 - D_S \leq 4$, where D_S is the surface fractal dimension, $2 \leq D_S \leq 3$.

It should be emphasized that a common property for all the samples under study is that three various q ranges exist, where the behaviors of the SANS cross section $d\Sigma(q)/d\Omega$ are significantly different. In particular, in the range $0.0025 < q < 0.015$ Å^{-1} the scattering cross section for all the samples satisfies the power law q^{-n}. The exponent n values found from the slope of the straight-line parts of the curves plotted in log-log scale (see Figs. 1 and 2) lie in the range from 3.4 to 3.7 (see Table I). This corresponds to the scattering from the fractal surface with the dimension $2.3 < D_S = 6 - n < 2.6$.

Deviations from the power law q^{-n} are observed for all the samples (sonicated and nonsonicated) both at lower and higher values of momentum transfer. For q smaller than 0.0015 Å^{-1}, such a deviation is caused by approaching the Guinier regime, where the scattering is determined by the maximum size R_c of independently scattering inhomogeneities. Analysis of the curve's slopes in Guinier region ($\ln[d\Sigma(q)/d\Omega]$ versus q^2) allows one to evaluate the values of the gyration radii R_g of such inhomogeneities as well as their characteristic size R_c. For instance, characteristic size of spheres can be calculated as $\boldsymbol{R}_C = \sqrt{5/3}\boldsymbol{R}_g$.[15]

At large q ($q > 0.025$ Å^{-1}) the so-called "shoulder of the curve" is observed indicating the presence of small inhomogeneities with characteristic size r_c. In this case function $d\Sigma(q)/d\Omega$ also exhibits Guinier behavior. Thus, the observed patterns are typical for scattering from systems possessing

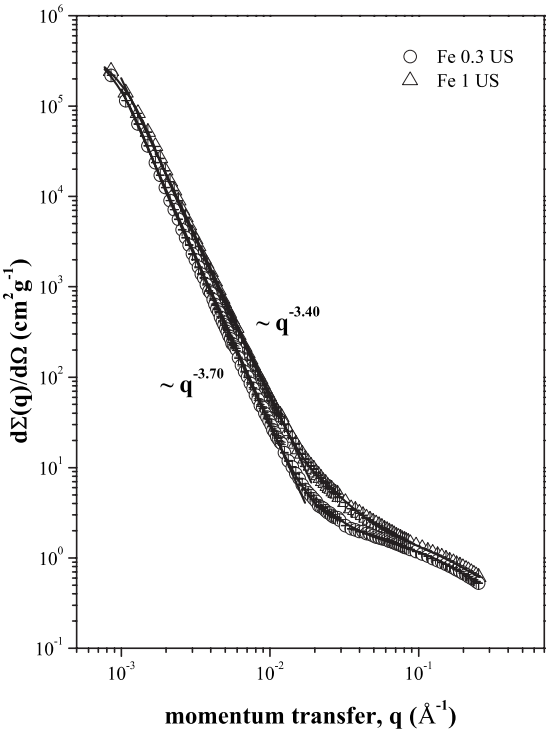

FIG. 2. SANS differential cross section $d\Sigma(q)/d\Omega$ for sonicated samples of amorphous $Fe(OH)_3 \cdot yH_2O$ xerogels obtained from $Fe(NO_3)_3$ solutions of different concentrations. Description of experimental data with Eq. (2) is given with firm lines. Corresponding n values are also indicated as q^{-n}.

disordered structure, for example, porous systems with fractal phase boundaries.[16] They indicate also that xerogels under investigation contain two types of scattering inhomogeneities with radically different characteristic sizes $R_c/r_c \approx 100$. These are likely large-scale aggregates consisting of primary particles. In turn, upper and lower self-similarity limits are determined as R_c and r_c values, respectively.

In view of this circumstance, we used the following expression to analyze scattering from amorphous iron (III) hydroxide xerogels over the entire q range:[17]

$$\frac{d\Sigma(q)}{d\Omega} = A_1 \cdot \exp\left(-\frac{q^2 R_g^2}{3}\right) + \frac{A_2(D_S)}{(\hat{q})^n} + A_3 \cdot \exp\left(-\frac{q^2 r_g^2}{3}\right). \tag{2}$$

Here, $\hat{q} = q/[\mathrm{erf}(qR_g/6^{1/2})]^3$—momentum q transferred, normalized to an error function $\mathrm{erf}(x)$. Such a procedure allows the cross section of scattering $d\Sigma(q)/d\Omega$ to be described correctly in the intermediate region between $qR_c < 1$ (Guinier approximation) and $qR_c \gg 1$ (q^{-n} asymptotics), where scattering from both surfaces and aggregates of characteristic size R_c contributes. The values of A_1 and A_3 are directly proportional to the number and the volume of inhomogeneities (aggregates and monomers, respectively) and to the density of their neutron scattering amplitudes.[18,19] Amplitude $A_2(D_S)$ depends on the fractal dimension of the system.[16]

It is well known that for porous materials consisting of two homogeneous phases A_2 is related to the phase-interface surface as[16]

$$A_2(D_S) = \pi\rho^2\Gamma(5 - D_S)\sin[(D_S - 1)(\pi/2)]N_0, \tag{3}$$

where N_0 is the characteristic of the fractal boundary, Γ is the gamma function, ρ_h is the solid-phase density, and ρ for a molecule containing several elements is defined as

$$\rho = \sum_i b_i N_i \frac{\rho_h N_A}{M}. \tag{4}$$

Here, N_A is the Avogadro constant, M is the molar mass, b_i is the scattering length for the ith element in the molecule, and N_i is the number of atoms of this element. The constant N_0 in Eq. (3) is related to the specific surface (S_0) of the surface fractal as $S_0 = N_0 \cdot r^{2-D_s}$, where r^{2-D_s} is determined by the length of the yardstick. For smooth surfaces, $D_S = 2$ and $N_0 = S_0$.

To obtain the final results, expression [Eq. (2)] was convolved with the setup resolution function. The experimental curves of the differential cross section $d\Sigma(q)/d\Omega$ versus q

TABLE I. Parameters of mesostructure of $Fe(OH)_3$ amorphous xerogels obtained from SANS measurements.

	Sample			
Parameter	Fe-0.3C	Fe-0.3US	Fe-1C	Fe-1US
ρ_h(g/cm^3)	1.62 ± 0.05	1.71 ± 0.05	1.31 ± 0.05	1.6 ± 0.05
T	0.506 ± 0.002	0.510 ± 0.002	0.424 ± 0.002	0.459 ± 0.002
$A_1 \times 10^5$(cm^2/g)	6.39 ± 0.04	6.31 ± 0.04	6.15 ± 0.02	5.44 ± 0.03
R_g(Å)	2080 ± 20	2140 ± 20	1680 ± 20	1890 ± 20
$A_2 \times 10^{-6}$(1/cm^2 g)	1.5 ± 0.1	0.9 ± 0.1	2.1 ± 0.2	4.0 ± 0.2
D_s	2.32 ± 0.04	2.30 ± 0.04	2.43 ± 0.04	2.60 ± 0.04
A_3(cm^2/g)	1.17 ± 0.01	1.18 ± 0.01	1.74 ± 0.01	1.72 ± 0.01
r_g(Å)	12.8 ± 0.1	13.1 ± 0.1	15.9 ± 0.1	16.4 ± 0.1
N_0(cm^{D_s}/g)	740 ± 30	720 ± 30	500 ± 20	65 ± 3
S_0(m^2/g)	13 ± 0.5	10 ± 0.5	51 ± 2	103 ± 4

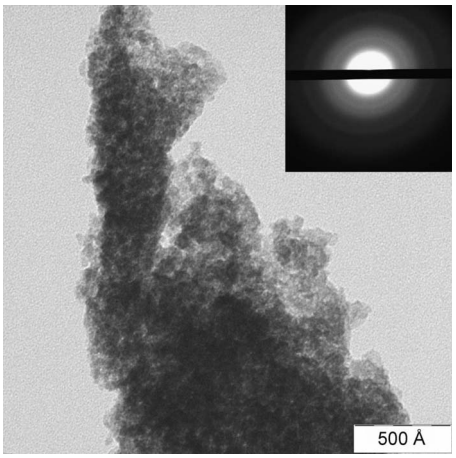

FIG. 3. Transmission electron microscopy of Fe-1C sample. Corresponding electron-diffraction pattern is presented in the inset.

were processed by the least mean squares method over the entire q range under investigation. The results of this analysis are given in Table I.

The obtained values of gyration radii ($\boldsymbol{r_g}$) of primary particles were used to estimate their mean size of individual particles ($\boldsymbol{D}$) supposing that they have a spherical shape. Calculations were made using previously mentioned relationship $D=\sqrt{5/3}\cdot 2r_g$. Resulted $\boldsymbol{D}$ values were 33–34 Å for samples obtained from 0.3 M solutions and 41–42 Å for samples obtained from 1 M solutions. Additional information on the microstructure and mesostructure of xerogels was obtained using transmission electron microscopy. The data give the evidence that all samples consist of strongly aggregated amorphous particles, which size is about 30–50 Å (Fig. 3). Thus, electron microscopy confirms SANS data and this fact practically proves the validity of model used to fit data [Eq. (2)].

Values of S_0 and N_0 were estimated by standard procedure[16] used by us earlier in the study of the mesostructure of amorphous xerogels of hydrous zirconia.[11] The constant N_0 can be determined from the small-angle scattering data in the large q limit,[16]

$$N_0 = \frac{\lim_{q\to\infty}\left[q^{6-D_S}\dfrac{d\Sigma(q)}{d\Omega}\right]}{\pi\rho^2\Gamma(5-D_S)\sin[(D_S-1)\pi/2]}. \tag{5}$$

All corresponding data are also given in Table I.

To analyze quantitatively the influence of ultrasonic treatment on the structure of amorphous $Fe(OH)_3\cdot yH_2O$ xerogels we have compared the scattering from sonicated and nonsonicated samples. The results of such a comparison are presented in Fig. 4 as a difference in scattering between these samples,

$$\frac{d\Sigma_{Dif}(q)}{d\Omega} = \frac{d\Sigma_C(q)}{d\Omega} - \frac{d\Sigma_{US}(q)}{d\Omega}. \tag{6}$$

According to these data, it is clear that this difference is positive over the entire q range regardless of the concentration of initial iron (III) nitrate solutions. This indicates that

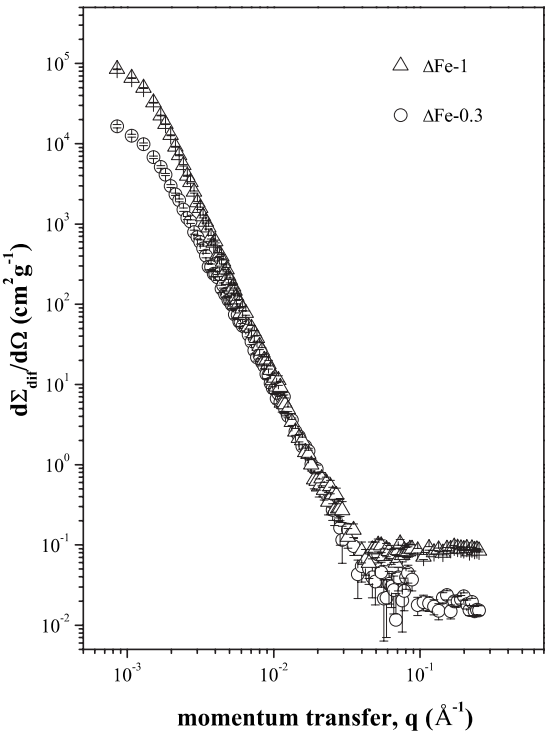

FIG. 4. Differences between SANS data for sonicated and nonsonicated samples [ΔFe-1—samples obtained from 1 M $Fe(NO_3)_3$ solution; ΔFe0.3—samples obtained from 0.3 M $Fe(NO_3)_3$ solution].

sonication results in formation of more homogeneous xerogels. This result is in a good agreement with the values of transmission of a neutron beam (T) presented in Table I. Parameter T is inversely proportional to integral scattering cross section and its growth also indicates that fluctuations of nuclear density in sonicated samples are smaller than in control ones.

Analysis of structural parameters given in Table I shows that the mesostructure of xerogels depends notably on the concentration of initial iron (III) nitrate solutions. It can be clearly seen that the increase in the concentration leads to decrease in clusters size and, on the contrary, to the increase in primary particles size. The second conclusion arising from these data is that the increase in the concentration also results in the significant increase in surface fractal dimension of aggregates. Thus we can conclude that homogeneity of xerogels falls with the increase in concentration of an initial solution.

Moreover, these data show that characteristic sizes of aggregates R_c are substantially lower (approximately fivefold) than the size of a collapsing cavitation bubble. Thus, basing on commonly accepted point of view, ultrasonication should not significantly affect the structure of the gel. Nevertheless our results indicate that ultrasonic treatment leads to the growth of the size R_c of aggregates of primary particles. This conclusion agrees with previously discussed differential SANS curves. It should be mentioned that the increase in R_c under ultrasonication is more significant in the case of gels obtained from 1 M $Fe(NO_3)_3$ solution. It should be also emphasized that in the case of concentrated solutions ultrasoni-

cation results also in notable increase in fractal dimension of a resulting xerogel (see Table I).

Thus, basing on the results obtained we can suggest how the mesostructure of hydroxide gels is formed under sonication. Microjets of liquid being formed during the collapse of cavitation bubbles capture aggregates of iron (III) hydroxide colloid particles and the frequency of their collisions grows notably. This leads to the changes in the internal structure and particle size of resulting gels. It is obvious that this effect becomes more evident when sonication is applied to more concentrated suspensions of hydroxides.

IV. *IN SITU* CALORIMETRIC EXPERIMENTS

We have also performed *in situ* calorimetric experiments to find out whether the difference in xerogels structure induced by sonication will contribute to mechanism and kinetics of iron (III) oxide formation followed by their decomposition under hydrothermal conditions. The method applied was proved to be rather sensitive to distinguish similar samples with various prehistory by means of measuring their reactivity.[20]

Analysis of the heat generation curves recorded in course of calorimetric measurements directly under hydrothermal conditions indicates that only one noticeable exothermal stage is observed in the temperature range 30–210 °C in each case [Fig. 5(a)]. Total heat effects of the process obtained by integrating corresponding heat generation rate curves were found to be -12.46 ± 0.10 kJ/mol and -11.74 ± 0.10 kJ/mol for Fe-1C and Fe-1US samples, respectively.

Generally thermal decomposition of nonsoluble hydroxides in air or in an inert atmosphere proceeds as an endothermal process. In our case the resulting process is undoubtedly an exothermal one. Thus we can suppose that under hydrothermal conditions decomposition of iron (III) hydroxide is accompanied with immediate exothermal crystallization of freshly formed amorphous Fe_2O_3. Heat effect value of such crystallization is supposed to be much higher than that of hydroxide decomposition, so the resulting process turns out to be exothermal. It should be noted that such a behavior was previously observed in the course of the study of several transition-metal hydroxides decomposition, e.g., during hydrothermal decomposition of titanium hydroxide[20] and hafnium hydroxide.[21]

Comparing heat generation curves for Fe-1C and Fe-1US samples one can easily see that preliminary ultrasonic treatment does considerably affect the properties of iron (III) hydroxide gels. In particular, decomposition beginning for a sonicated sample takes place at a higher temperature ($\Delta T \approx 20$ °C), whereas the end of the process is nearly at the same temperature. As a result the exothermal peak registered for this sample is definitely narrower and has a distinct shape with almost linear rate increasing slope and very steep rate decreasing slope without any diffusive "tail." This is rather different from that for a nonsonicated sample, where the rate decreasing slope is prolonged and nonmonotonous. Furthermore, the full heat generation curve for Fe-1C sample contains a number of consecutive small sharp peaks at relatively low temperatures (up to ~80–110 °C) which are not observed at all for Fe-1US sample. These peaks are definitely of nonkinetic nature. They look like breaking the heat-capacity function due to some fast second-order phase transition or similar process. The real reason may be opening the closed domains under hydrothermal conditions. These domains could be formed at the precipitation stage and might

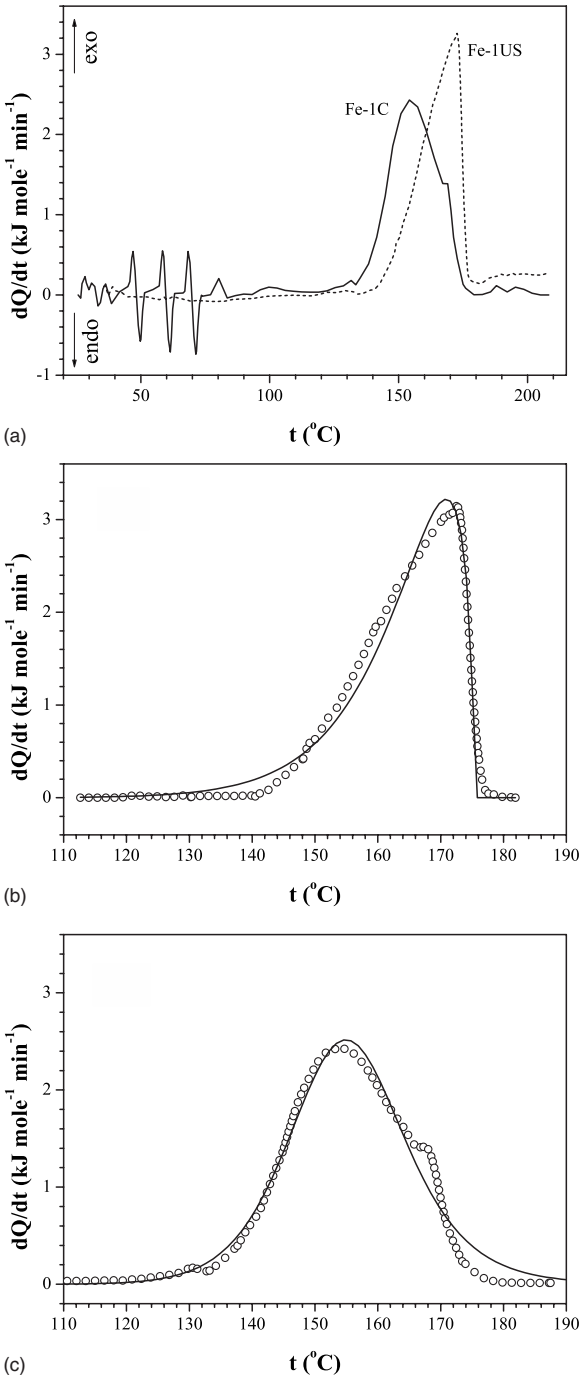

FIG. 5. *In situ* heat-flux calorimetry data (a) for iron hydroxide xerogels transformation under hydrothermal conditions [both gels obtained from 1 M $Fe(NO_3)_3$ solution, kinetic modeling results (b)—under ultrasonic treatment, and (c)—without ultrasonication]. Experimental (points) and calculated (lines) heat production rate curves of iron hydroxide xerogels transformation under hydrothermal conditions.

TABLE II. Results of kinetic analysis of iron (III) hydroxide xerogels hydrothermal decomposition.

	Fe-1C	Fe-1US
E_{a1}, kJ/mol	115.95[a]	115.95[a]
ln K_{01}, min^{-1}	9.932	8.425
N_1	1.00	1.00
E_{a2}, kJ/mol	115.95[a]	115.95[a]
ln K_{02}, min^{-1}	29.932	28.425
N_2	0.500	0.300
N_3	1.50	0.333
Q^{∞}, kJ/mol	12.46[b]	11.74[b]

[a]Results of independent experiment.
[b]Experimental value.

contain small amounts of trapped ions including NH_4^+, NO_3^-, and even nonprecipitated Fe^{3+} ions that could not be removed at the washing stage. Opening the domains and interaction of the trapped ions with hydrothermal solution at the elevated temperature should cause the effect observed. Sonication of gels at the stage of precipitation obviously prevents formation of such closed domains and leads to formation of xerogels with a more uniform structure.

The difference in heat effect values is also noticeable, the greater heat effect for the nonsonicated sample indicates that it possesses a greater free energy being released through hydrothermal decomposition-crystallization, as the final state can be considered the same for both samples. This is also in favor of a more uniform xerogel structure that is formed upon sonication.

To obtain an additional information on the mechanism of iron (III) hydroxide xerogels hydrothermal decomposition we have performed a comparative formal-kinetic analysis of both heat generation curves. Kinetic data are not enough for a rigorous analysis, yet it is still possible to provide some semiquantitative conclusions. We have applied a generalized autocatalysis model as the peak shapes allow us to suppose it and the validity of namely this kind of a model was strictly proved for a similar process of titanium oxide formation,[20]

$$\frac{dQ}{d\tau} = \frac{d\alpha}{d\tau} Q^{\infty}, \tag{7}$$

$$\frac{d\alpha}{d\tau} = K_1(1-\alpha)^{N_1} + K_2\alpha^{N_2}(1-\alpha)^{N_3}, \tag{8}$$

where Q^{∞} is the total heat effect of reaction; α is the degree of conversion; N_1, N_2, and N_3 are parameters of the full autocatalysis model; K_1 and K_2 are the rate constants in the model of full autocatalysis ($K_i = K_{0i} \cdot \exp\{-E_{ai}/RT\}$).

The following basic parallel processes are considered within the formal-kinetic model: (a) $Fe(OH)_3 \cdot yH_2O \rightarrow 1/2Fe_2O_3 + (1.5+y)H_2O$ [N-order formal model, first term in Eq. (8)] and (b) $Fe(OH)_3 \cdot yH_2O + 1/2Fe_2O_3 \rightarrow Fe_2O_3 + (1.5+y)H_2O$ [autocatalytic formal model, second term in Eq. (8)].

As the general autocatalysis model contains a lot of parameters that are not totally independent and generally the solution might not be the only one—the following procedure was applied. E_a value was reliably determined from independent experiments on iron hydroxide gel decomposition under hydrothermal conditions where no self-acceleration was observed and this value was used in the model. N_1 parameter of the first, initiating stage was fixed and equal to 1. Heat effect values were the experimental ones. Four other parameters have been calculated in course of solving the inverse kinetic task. The solution was unique. More details on methodology and related aspects of kinetic modeling are given in Ref. 22.

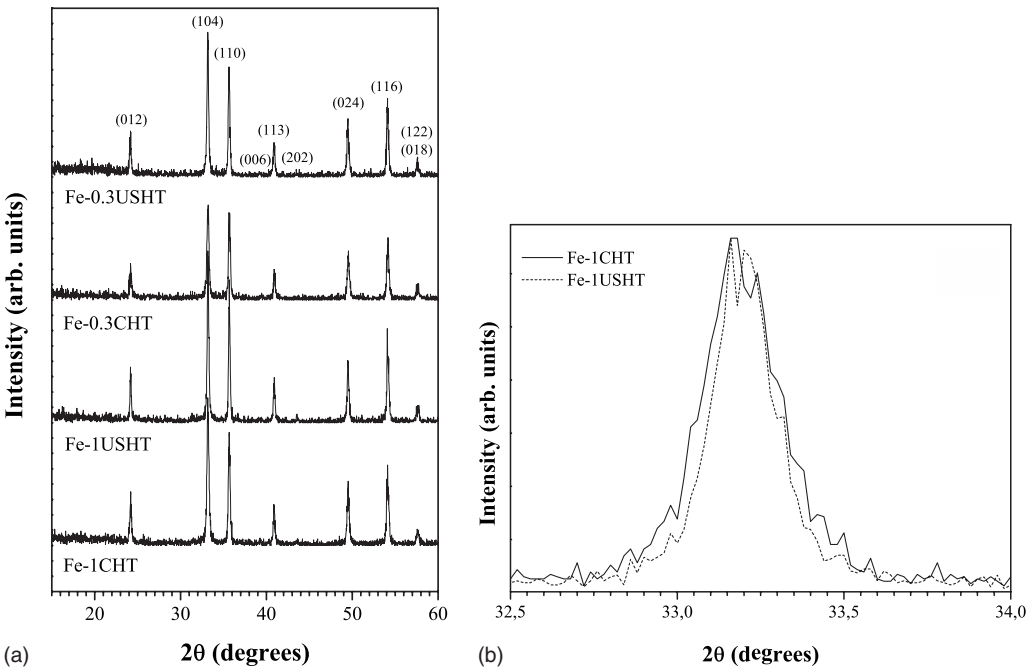

FIG. 6. XRD of xerogel samples after hydrothermal treatment.

The results of kinetic analysis (model parameters for each case obtained in the result of solving the inverse kinetic task) are given in Table II. A good coincidence between experimental and calculated heat production rate curves has been reached for both samples. Modeling results are illustrated in Figs. 5(b) and 5(c).

According to the results obtained in course of kinetic analysis, the process of iron (III) hydroxide xerogels hydrothermal decomposition is mostly run according to an autocatalytic route [the second term in rate Eq. (8)]. Comparison of N_2 and N_3 parameters values allows one to conclude that the sonicated sample is decomposed with less self-acceleration and far less diffusive braking. These peculiarities also confirm a more uniform character of Fe-1US sample decomposition-crystallization.

Thus, analysis of heat-flux calorimetry data indicates that ultrasonic treatment of iron (III) hydroxide gel results in formation of a noticeably more homogeneous sample which is decomposed autocatalytically in one definite stage. Such a conclusion is in a good agreement with the results of SANS measurements confirming the same changes in the mesostructure.

It is obvious that the differences in hydrothermal dehydration process of sonicated and nonsonicated iron hydroxide xerogels can contribute to any properties of the resulting Fe_2O_3. In order to obtain the corresponding data we have performed hydrothermal processing of these samples. Temperature (160 °C) and duration (5 h) of hydrothermal treatment were chosen basing on the data obtained from heat-flux calorimetry.

According to XRD data [Fig. 6(a)] hydrothermal treatment under selected conditions leads to the formation of well crystalline α-Fe_2O_3. Transmission electron microscopy (Fig. 7) has shown that Fe_2O_3 powders consist of weakly aggregated and relatively small particles with average size of approximately 500–1000 Å. These data are in a good agreement with the crystallite size values estimated using Scherrer equation (400–600 Å). It should be emphasized that for all the samples obtained from sonicated iron hydroxide xerogels mean particle sizes are notably larger than for control ones. For instance, particle sizes for iron (III) oxide obtained from Fe-0.3C, Fe-1C, Fe-0.3US, and Fe-1US samples are 420 ± 30, 400 ± 20, 500 ± 30, and 600 ± 30 Å, respectively [Fig. 6(b)]. This fact can also be considered as an additional argument in favor of a higher homogeneity of ultrasonicated xerogel samples.

Transmission electron microscopy data evidence also that resulting hematite particles are mesoporous (see Fig. 7). The size of pores estimated roughly using TEM was found to be 30–50 Å.

Formation of mesoporous nanopowders of metal oxides under hydrothermal conditions was observed elsewhere.[3,23,24] The mechanism of nanopore formation is probably connected with adsorption of water molecules and ions (e.g., NH_4^+, NO_3^-) on the surface of metal hydroxides. It is obvious that complete removal of such species is very difficult even after thorough washing or sonication of an amorphous precipitate. During hydrothermal treatment adsorbate is partly removed but partly trapped in the bulk of growing particles. As a result formation of nanocavities filled with mother liquor takes place. Nevertheless, to the best of our knowledge the mechanism of mesoporous metal oxides formation under hydrothermal conditions is poorly discussed in literature and deserves a more thorough investigation.

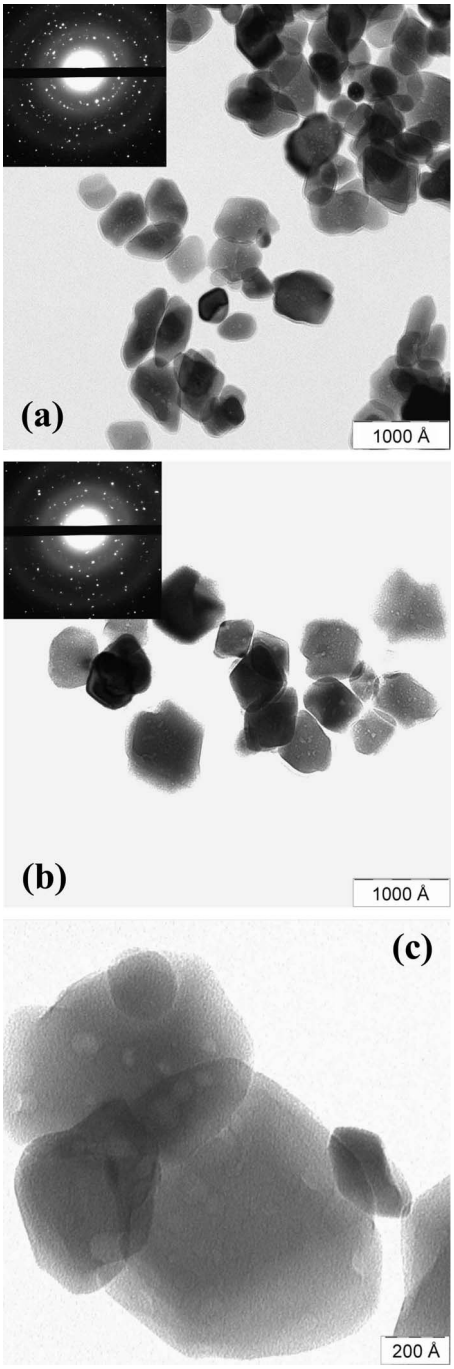

FIG. 7. Transmission electron microscopy of samples obtained after hydrothermal treatment of iron hydroxide xerogels: (a) Fe-1CHT and [(b) and (c)] Fe-1USHT.

V. SUMMARY

Influence of high intensity ultrasonic treatment on the structure of amorphous iron (III) hydroxide xerogels was

studied. Contrary to the commonly accepted point of view that ultrasonication should not significantly affect the structure of the gels, our results indicate the significant changes in their mesostructure under ultrasonic treatment. It has been shown that sonication leads to the increase in homogeneity of xerogels in mesoscopic range and, on the other hand, to the increase in the size of aggregates of $Fe(OH)_3$ primary particles as well as to the increase in the surface fractal dimension. It was also established that ultrasonically induced changes in mesostructure of xerogels greatly affect their subsequent transformation into nanocrystalline iron (III) oxide under hydrothermal conditions.

ACKNOWLEDGMENTS

This work was supported by RFBR (Grants No. 06-03-33042 and No. 07-02-00290) and FASI (State Contracts No. 40.012.1.1.1149 and No. 02.513.11.3352). V.K.I., G.P.K., and S.V.G. would like to thank GKSS Forschungszentrum for hearty welcome.

[1] A. Gedanken, Ultrason. Sonochem. **11**, 47 (2004).
[2] K. S. Suslick, Annu. Rev. Mater. Sci. **29**, 295 (1999).
[3] A. Ye. Baranchikov, V. K. Ivanov, and Yu. D. Tretyakov, Russ. Chem. Rev. **76**, 133 (2007).
[4] P. E. Meskin, V. K. Ivanov, A. E. Barantchikov, B. R. Churagulov, and Y. D. Tretyakov, Ultrason. Sonochem. **13**, 47 (2006).
[5] E. A. Neppiras, Phys. Rep. **61**, 159 (1980).
[6] M. A. Margulis, Physics-Uspekhi **43**, 259 (2000).
[7] D. Chaumont, A. Craievich, and J. Zarzycki, J. Non-Cryst. Solids **147-148**, 41 (1992).
[8] M. C. Barrera-Solano, N. de la Rosa-Fox, and L. Esquivias, J. Non-Cryst. Solids **147-148**, 194 (1992).
[9] D. R. Vollet, W. C. de Castro, D. A. Donatti, and A. Ibañez Ruiz, Phys. Status Solidi A **202**, 411 (2005).
[10] D. A. Donatti, D. R. Vollet, A. Ibañez Ruiz, A. Mesquita, and T. F. P. Silva, Phys. Rev. B **71**, 014203 (2005).
[11] G. P. Kopitsa, V. K. Ivanov, S. V. Grigoriev, P. E. Meskin, O. S. Polezhaeva, and V. M. Garamus, JETP Lett. **85**, 122 (2007).
[12] A. I. Benin, A. A. Kossoy, and F. Yu. Sharikov, J. Therm. Anal. **38**, 1167 (1992).
[13] S. Yang and A. Navrotsky, Microporous Mesoporous Mater. **52**, 93 (2002).
[14] W. Schmatz, T. Springer, J. Schelten, and K. Ibel, J. Appl. Crystallogr. **7**, 96 (1974).
[15] P. W. Schmidt, in *Modern Aspects of Small-Angle Scattering*, edited by H. Brumberger (Kluwer Academic, Dordrecht, 1995), pp. 1–56.
[16] H. D. Bale and P. W. Schmidt, Phys. Rev. Lett. **53**, 596 (1984).
[17] G. Beaucage, J. Appl. Crystallogr. **28**, 717 (1995).
[18] A. Guinier, G. Frournet, C. B. Walker, and K. L. Yudowitch, *Small-Angle Scattering of X-rays* (Wiley, New York, 1955), p. 17.
[19] A. Guinier, Ann. Phys. **12**, 161 (1939).
[20] F. Yu. Sharikov, V. K. Ivanov, Yu. V. Sharikov, and Yu. D. Tret'yakov, Russ. J. Inorg. Chem. **51**, 1841 (2006).
[21] P. E. Meskin, F. Yu. Sharikov, V. K. Ivanov, B. R. Churagulov, and Y. D. Tretyakov, Mater. Chem. Phys. **104**, 439 (2007).
[22] A. Kossoy and Yu. Akhmetshin, Process Saf. Prog. **26**, 209 (2007).
[23] Yu. V. Kolen'ko, V. D. Maximov, A. V. Garshev, P. E. Meskin, N. N. Oleynikov, and B. R. Churagulov, Chem. Phys. Lett. **388**, 411 (2004).
[24] M. N. Rumyantseva, V. K. Ivanov, A. S. Shaporev, Yu. M. Rudyi, V. V. Yushchenko, J. Arbiol, and A. M. Gas'kov, Russ. J. Inorg. Chem. **54**, 163 (2009).